
Article:
Naydenov, Genadi Antonov, Hasnip, Philip James orcid.org/0000-0002-4314-4093, Probert, Matthew Ian James orcid.org/0000-0002-1130-9316 et al. (1 more author) (2019) Huge power factor in p-type half-Heusler alloys NbFeSb and TaFeSb. Journal of physics : Materials. 035002.

https://doi.org/10.1088/2515-7639/ab16fb

JPhys Materials

PAPER • OPEN ACCESS

Huge power factor in p-type half-Heusler alloys NbFeSb and TaFeSb

JPhys Materials

OPEN ACCESS

RECEIVED
10 January 2019

REVISED
29 March 2019

ACCEPTED FOR PUBLICATION
8 April 2019

PUBLISHED
3 June 2019

PAPER

Huge power factor in p-type half-Heusler alloys NbFeSb and TaFeSb

G A Naydenov, P J Hasnip, V K Lazarov and M I J Probert

Department of Physics, University of York, York YO10 5DD, United Kingdom

E-mail: gan503@york.ac.uk

Keywords: thermoelectric materials, half-Heusler alloys, power factor, dft modelling, figure of merit, Seebeck coefficient

Supplementary material for this article is available online

Abstract

NbFeSb is a promising thermoelectric material which according to experimental and theoretical studies exhibits a high power factor of up to 10 mW m^{-1} K^{-2} at room temperature and ZT of 1 at 1000 K. In all previous theoretical studies, κ_{latt} is calculated using simplified models, which ignore structural defects. In this work, we calculate κ_{latt} by solving the Boltzmann transport equation and subsequently including the contributions of grain boundaries, point defects and electron–phonon interaction. The results for κ_{latt} and ZT are in excellent agreement with experimental measurements. In addition, we investigate theoretically the thermoelectric properties of TaFeSb. The material has recently been synthesised experimentally, thus confirming the theoretical hypothesis for its stability. This encourages a full-scale computation of its thermoelectric performance. Our results show that TaFeSb is indeed an excellent thermoelectric material which has a very high power factor of 16 mW m^{-1} K^{-2} at room temperature and ZT of 1.5 at 1000 K.

1. Introduction

NbFeSb is a half-Heusler intermetallic compound which has recently attracted a lot of attention as a potential thermoelectric material due to its ecologically friendly properties and the relatively high earth abundance of Nb and Fe. NbFeSb alloys are reported to have a large power factor of up to 10 mW m^{-1} K^{-2} [1], beating some of the best thermoelectrics, e.g. Bi_2Te_3. However, their thermal conductivity is also a lot higher than Bi_2Te_3 [1–3]. The high thermal conductivity of NbFeSb is phonon dominated and this provides much room for improvement of the current thermoelectric figure of merit maximum of $ZT = 1$ at 1000 K.

The thermoelectric figure of merit is given by the equation $ZT = S^2\sigma T/\kappa$ and several theoretical and experimental studies which aim to optimise the thermal conductivity (κ) as well as the Seebeck coefficient (S) and electrical conductivity (σ) have been conducted in the past couple of years [1, 2, 4–10]. This optimisation is done by p-type doping with Ti, Hf and Zr for Nb or Sn for Sb. Such an approach maximises the power factor by fine tuning of the doping levels and decreases the lattice thermal conductivity by enhancing the phonon scattering due to the mass difference between the dopant and host atoms. To date, the best NbFeSb results are obtained by Ti doping [1] due to the large mass difference between Ti and Nb. The mass difference can be further enhanced if Nb is substituted with a heavier but chemically similar element like Ta, which is something that has not yet been thoroughly investigated.

The first aim of this study is to compute the lattice thermal conductivity (κ_{latt}) of NbFeSb using the semi-classical Boltzmann transport equation (BTE) and compare the obtained theoretical thermoelectric (TE) results to experimental measurements. The second aim is to use the same approach and calculate the TE properties of a compound very similar to NbFeSb, namely TaFeSb. A theoretical study by Bhattacharya and Madsen [9] reports that TaFeSb is a stable compound which can also be doped with Ti in a similar way to NbFeSb. A very recent experimental study by Zhu *et al* [11] investigates extensively the phase stability of the compound and provides an XRD pattern after the successful experimental synthesis of TaFeSb. The main interest in TaFeSb comes from the fact that it has the same number of valence electrons as NbFeSb, while Ta has almost twice the mass of Nb. This suggests that TaFeSb should have the same good electronic TE properties as NbFeSb. In addition, the heavier Ta

should also lead to an increase in the scattering strength in doped TaFeSb due to point defects (PD) and thus decrease κ_{latt}. As a result, TaFeSb may be expected to have a significantly higher ZT than NbFeSb but until now there have been no full-scale theoretical studies on the pure TaFeSb compound to confirm this hypothesis. Zeeshan *et al* [12] investigates the thermoelectric properties of TaFeSb but without computing the electron relaxation time or including the additional phonon scattering mechanisms. Another recent study conducted by Yu *et al* [8] investigates the effect of Ta but in NbFeSb systems. Hence, this is clearly a very hot topic and there is a strong need for a full study of the thermoelectric properties of TaFeSb.

2. Methodology and theory

We split our calculations into two stages. We solve the electron BTE in the first stage and the phonon BTE in the second one. The energy distribution of the charge carriers and phonons is computed from first-principles.

2.1. DFT calculations and electronic TE properties

The first-principles calculations were performed with the CASTEP [13] code and the generalised gradient approximation Perdew–Burke–Ernzerhof (GGA-PBE) exchange-correlation functional [14]. On-the-fly ultrasoft pseudopotentials (C9 set) [15] were used with a plane-wave cut-off energy of 700 eV with a grid scale of size 2.0. A cubic unit cell, corresponding to four elementary rhombohedral cells, was used for all simulations. The Brillouin zone was sampled using a Monkhorst–Pack grid [16] with an $8 \times 8 \times 8$ $\vec{k}$-points mesh (equivalent to $\vec{k}$-points spacing of 0.021 $2\pi\text{Å}^{-1}$). The structure was fully optimised until pressure and energy were converged to 0.1 GPa and 0.02 meV/atom, respectively. Density of states (DOS) and partial density of states were analysed using the OptaDOS code [17].

Electronic transport properties were calculated using the semi-classical Boltzmann transport formalism as implemented in the BoltzTraP code [18]. The electronic eigenenergies required for the transport properties were calculated with CASTEP on a $48 \times 48 \times 48$ $\vec{k}$-points mesh, which was later interpolated on a 5 times denser mesh in BoltzTraP. The simulated half-Heusler alloys are isotropic and the Seebeck coefficient S, electrical conductivity σ and electron thermal conductivity κ_{el} can be evaluated as the average of the trace of the respective tensors. The final results are obtained as a function of the temperature (T) for 37 fixed doping levels from $n_h = 10^{18}$ cm^{-3} to $n_h = 10^{22}$ cm^{-3}. BoltzTraP calculates both electrical and electron thermal conductivity as σ/τ and κ_{el}/τ where τ is the relaxation time. We use the deformation potential (DP) theory to compute τ [19]. A more detailed explanation of the steps needed for calculating τ is provided in the supplementary materials.

2.2. Lattice thermal conductivity modelling

2.2.1. ShengBTE and thirdorder programs

The lattice thermal conductivity was calculated by solving the phonon BTE in ShengBTE, which as inputs requires the second order force constants (usually just called the 'force constants') and the anharmonicity (third order force constants) of the system. The second order force constants were obtained with CASTEP using density-functional perturbation theory for the phonons [20]. The calculations used the GGA-PBE exchange-correlation functional [14], on-the-fly norm-conserving pseudopotentials (NCP17 set) and a plane-wave cut-off energy of 2000 eV with a grid scale of size 2.0. The Brillouin zone was sampled using a Monkhorst–Pack [16] grid with an $5 \times 5 \times 5$ $\vec{k}$-points mesh (equivalent to $\vec{k}$-points spacing of 0.034 $2\pi\text{Å}^{-1}$). A $\vec{q}$-point grid of the same size and spacing was used for calculating the second order force constants.

The third order force constants were calculated using the finite-displacement supercell approach. The set of supercells and the reconstruction of the force constants was performed by the *thirdorder.py* script that is provided as part of the ShengBTE package. The *ab initio* calculations were done using CASTEP. The settings for these runs included: a $2 \times 2 \times 2$ cubic supercell, on-the-fly ultrasoft pseudopotentials (C9 set), a plane-wave cut-off energy of 600 eV with a grid scale of size 2.0 and a very fine energy per atom convergence tolerance of 2×10^{-10} eV.

ShengBTE computes the intrinsic lattice thermal conductivity κ_{int} due to 3P (three-phonon) processes. We have also included the effect of grain boundaries (GB), PD and electron–phonon (EP) interaction to the lattice thermal conductivity. More details on how this is done are given in the supplementary materials.

3. Results

The results are split into two subsections. The first one presents the calculations on the TE properties of NbFeSb. We start by following the well-established procedure of using BoltzTraP [18] to obtain the electronic properties of the material and then solve the phonon BTE using ShengBTE [21]. Furthermore, we build upon the method

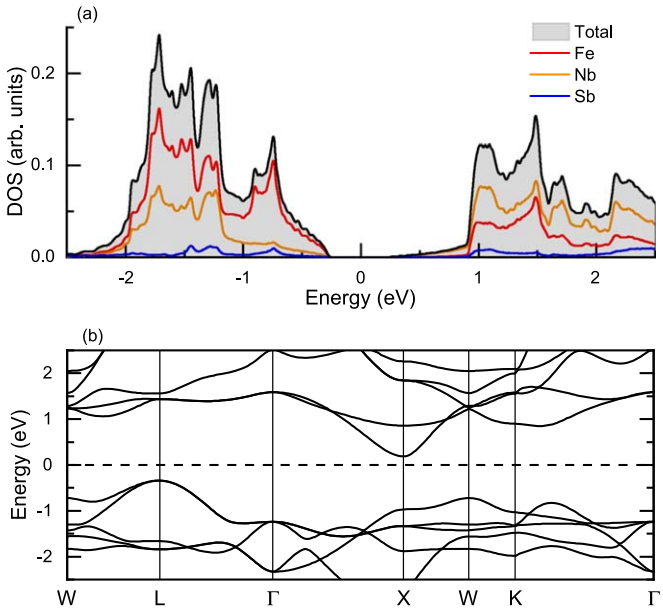

Figure 1. Density of states (a) and band structure (b) graphs of NbFeSb.

proposed by Hong *et al* [5] for the inclusion of PD and introduce the contributions of GB and EP interaction to the lattice thermal conductivity of NbFeSb. To the best of our knowledge, this is the first instance when the lattice thermal conductivity of NbFeSb is calculated by solving the BTE and including all these additional contributions. For this reason, the results are thoroughly compared to the available experimental data. The second section follows a similar layout but is focused on TaFeSb and the observed improvements in TE properties with respect to NbFeSb.

It is worth pointing out that BolzTraP calculates the TE properties at different doping levels by changing the chemical potential implicitly and hence the dopant atoms are not explicitly included. For this reason, the *p*-type compounds in electronic properties section are referred simply as NbFeSb and TaFeSb. However, the computation of the change in the lattice thermal conductivity due to PD requires knowledge of the atomic mass of the dopant atoms. In this case, the structures are referred as $Nb_{1-x}Ti_xFeSb$ and $Ta_{1-x}Ti_xFeSb$, with Ti being used for the *p*-type doping.

3.1. NbFeSb

3.1.1. Electronic structure

NbFeSb is a half-Heusler compound, which has a composition of XYZ, where X and Y are transition metals and Z is a main group element. The crystal structure is face-centred cubic, having space group $F\bar{4}3m$ (216). The lattice constant is calculated to be 5.96 Å, which agrees well with the experimental value of 5.95 Å [4]. The band structure and DOS are presented in figure 1. The figure shows that the conduction band minimum is at the Γ-point, whereas the valence band maximum is positioned at the L-point. The magnitude of the formed indirect band gap (ϵ_g) is 0.53 eV, which is in an excellent agreement with other theoretical [1, 5, 6] ($\epsilon_g = 0.52$ and 0.53 eV) and experimental [1] ($\epsilon_g = 0.51$ eV) studies. The partial DOS show that Fe and Nb are the main contributors to states around the Fermi level. This means that the power factor is mainly affected by Fe and Nb rather than Sb.

3.1.2. Electronic TE properties

The parameters needed to calculate the electron relaxation time for bulk NbFeSb are given in table 1. These include the DP (V_{DP}), effective mass of the charge carriers (m^*), carrier mobility (μ) and relaxation time (τ). The elastic constants are given in table S1 in the supplementary materials available online at stacks.iop.org/JPMATER/2/035002/mmedia. The values of the parameters obtained for holes are slightly higher, but within the margin of error, than the ones obtained experimentally by He *et al* [1] and Fu *et al* [4]. The experimental measurements have been performed on doped systems which exhibit structural defects. Therefore, a slight overestimate is to be expected when the results are compared to the modelled perfect bulk system. To the best of our knowledge there are no experimental results on the electron parameters. However, the electron values presented in table 1 agree extremely well with the theoretical prediction of Hong *et al* [5]. The magnitude of the DP constant for holes ($V_{DP} = -13.98$ eV) is lower than the one for electrons ($V_{DP} = -14.53$ eV). This can be

Table 1. Parameters needed for electron and hole τ calculations of NbFeSb. These include the deformation potential (V_{DP}), effective mass of charge carriers (m^*), carrier mobility (μ) and relaxation time (τ) at 300 K for electrons and holes.

Carrier type	V_{DP} (eV)	$m^*(m_e)$	μ (cm^2 V^{-1} s^{-1})	τ (fs)
Holes	−13.98	1.65	28.02	26.23
Electrons	−14.53	0.35	1 243.93	247.54

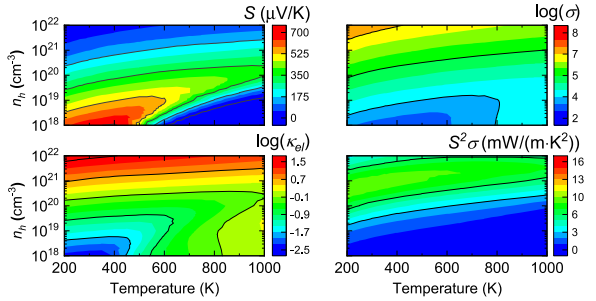

Figure 2. Colour maps of the electronic TE properties of *p*-type NbFeSb. The magnitude of the electrical conductivity σ (top right) and electronic thermal conductivity κ_{el} (bottom left) is given on a log scale. A maximum power factor (bottom right) value of PF $= S^2\sigma$ $= 9.15$ mW m^{-1} K^{-2} is obtained at 300 K and $n_h = 7 \times 10^{20}$ cm^{-3} ($x = 0.037$).

explained by the different dispersion of the valence and conduction bands. The bottom conduction band is more dispersive than the top valence band, and the applied strain has a smaller effect on the flatter bands. Due to the difference in the dispersion of the bands, the effective mass of electrons $m_{el}^* = 0.35(m_e)$ is much smaller than that of the holes $m_h^* = 1.65(m_e)$. This results in a much lower mobility ($\mu_h = 28.02$ cm^2 V^{-1} s^{-1}) of the heavier holes and a lower relaxation time of $\tau_h = 26.23$ fs at 300 K. This value of the relaxation time, with the included temperature dependence of $\tau \propto 1/T^{3/2}$ is used to post-process the results obtained from BoltzTraP for the *p*-type behaviour of NbFeSb.

The calculated thermoelectric properties of *p*-type NbFeSb are shown in figure 2. All quantities agree very well with results obtained in the other theoretical studies [5, 6]. It can be seen that the Seebeck coefficient (top left graph) reaches values up of 700 μV K^{-1} at low temperature (around 300 K) and at extremely small doping levels (between 0.04 and 0.004% hole concentration). When the doping concentration is increased to the experimental values of $x = 0.04$ ($n_h = 8 \times 10^{20}$ cm^{-3}) the Seebeck coefficient becomes 129 μV K^{-1} and 266 μV K^{-1} at 300 K and 1000 K, respectively. These values are slightly lower than the experimental results obtained by Fu *et al* [4] ($S = 150$ μV K^{-1} and 285 μV K^{-1} at 300 K and 1000 K, respectively) and He *et al* [1] ($S = 175$ and 300 μV K^{-1} at 300 and 1000 K, respectively). It is worth mentioning, however, that a lower doping level in the theoretical model of $n_h = 6 \times 10^{20}$ cm^{-3} ($x = 0.03$) yields identical results to the experimental ones obtained for $x = 0.04$ by Fu *et al* [4]. This could mean that an $x = 0.04$ does not strictly correspond to 8×10^{20} cm^{-3} hole concentration in the experimental samples, and some of the holes could be compensated. In fact, Fu *et al* [4] results show that a doping level of $x = 0.04$ corresponds more to $n_h = 6 \times 10^{20}$ cm^{-3} rather than $n_h = 8 \times 10^{20}$cm^{-3}, as the theory suggests. For simplicity, however, we use the theoretical relation between x and n_h (volume $= x/n_h$), where the volume is theoretically calculated to be 52.86×10^{-24} cm^3.

The electrical conductivity σ and electronic thermal conductivity κ_{el} also agree very well with other theoretical studies [5, 6], but are slightly larger than found in experiment [1, 4]. There are a few reasons for this discrepancy. As already mentioned, the carrier mobility of the perfect crystal is expected to be higher than μ of the doped compounds, hence τ and σ are also larger. Second, the temperature dependence of τ is no longer proportional to $T^{-3/2}$ at temperature <450 K [1, 4]. Finally, the constant relaxation time approximation lacks dependence on the chemical potential, which means that additional scattering events are not captured when the doping levels are increased. Thus, σ and κ_{el} tend to be overestimated at high doping levels. Nevertheless, the current model for τ is a computationally inexpensive approach that allows us to calculate values for σ and κ_{el}, which agree relatively well with both theoretical and experimental studies.

The highest value of the power factor PF $= S^2\sigma$ is obtained at $n_h = 7 \times 10^{20}$ cm^{-3} ($x = 0.037$) and yields PF $= 9.15$ and 5.23 mW m^{-1} K^{-2} at 300 K and 1000 K, respectively. This result is very close to the key result of He *et al* [1] study of PF $= 10.6$ mW m^{-1} K^{-2} at room temperature and $x \approx 0.05$. In general, the power factor values remain consistent with the experimental measurements up to $n_h = 2 \times 10^{21}$ cm^{-3} ($x = 0.1$). Beyond that value, the theoretical prediction starts to overestimate the experimental results by values up to

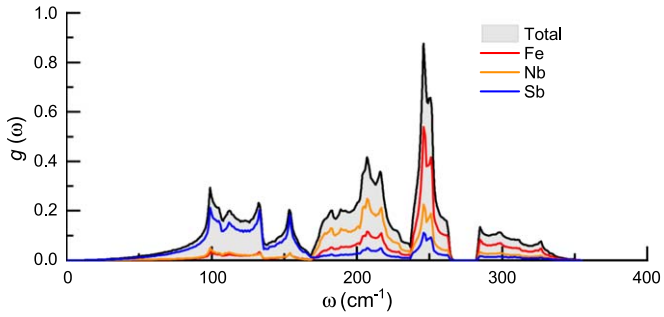

Figure 3. Phonon density of states of NbFeSb.

$\approx$2 mW m^{-1} K^{-2} when one reaches $x = 0.3$. Such behaviour is also noticed by the other theoretical studies mentioned before. The reason for this could be either the constant relaxation time approximation, or the fact that the heavy doping significantly changes the electronic structure of the system. However, as shown experimentally, NbFeSb exhibits its best thermoelectric performance at around $x = 0.05$, and this region is accurately modelled by the current theoretical approach.

3.1.3. Lattice thermal conductivity

The phonon DOS are presented in figure 3. The data is in a good agreement with the results obtained by Hong *et al* [5] and Zeeshan *et al* [12] and as there are no imaginary frequencies the structure is mechanically stable. The phonon DOS can be split into three regions. The first one is at low frequency, $\omega < 170$ cm^{-1} where the lattice vibrations are primarily due to Sb atoms. The dominant contributor to the phonon DOS for $170 < \omega < 230$ cm^{-1} is Nb, whereas for $\omega > 230$ cm^{-1} lattice vibrations are predominantly due to Fe with a small contribution from Nb. The Nb atomic vibrations have the biggest frequency spread among the constituents of the material. In addition, the mass difference between Nb and the dopant atoms (here assumed to be Ti) leads to an increase in the scattering strength. Thus, the lattice thermal conductivity κ_{latt} of NbFeSb can be reduced significantly by doping. Our results show the clear presence of a phonon gap at $\omega \approx 275$ cm^{-1}, something which is not observed either by Hong *et al* or Zeeshan *et al* [12]. The reason for this discrepancy comes from the choice of the $\vec{q}$-point grid for the phonon calculations. The phonon DOS converges slowly and the gap only becomes apparent when the $\vec{q}$-point mesh is at least $3 \times 3 \times 3$ or equivalently a spacing of 0.056 2πÅ^{-1}.

Next we focus on the estimated value for the lattice thermal conductivity and how different contributions affect it. The intrinsic value of κ_{latt} obtained from ShengBTE is 21.82 and 6.49 W m^{-1} K^{-1} at 300 and 1000 K, respectively. This agrees very well with the theoretical result obtained by Hong *et al* [5] but is a bit higher than the experimental measurements [1, 4]. The main reasons for this discrepancy is the fact that there are no defects such as GB, PD or dopant atoms in the modelled structure. To correct this, we include the effect of all mentioned impurities by using Klemens' model [22] and calculating the impact on the intrinsic value obtained from ShengBTE.

The study conducted by He *et al* reports that the size of the GB in NbFeSb varies between 0.3 and 4.5 μm, depending on the hot pressing temperature. Figure 4 shows how the lattice thermal conductivity of phonons with a given mean free path changes at room temperature when GB are included in the theoretical model. The graph illustrates the effect of GB (L_{GB}) by considering two different average sizes of $L_{\mathrm{GB}} = 4.5$ and 0.5 μm. Blue circles represent the intrinsic values of κ_{latt} and it can be seen that $L_{\mathrm{GB}} = 4.5$ μm, illustrated with black and white squares, have an almost negligible impact on κ_{latt}. However, there is a noticeable change in κ_{latt} when the size of the GB is reduced to 0.5 μm (orange triangles), and the accumulated value of κ_{latt} becomes 18.84 W m^{-1} K^{-1}. For completeness, $L_{\mathrm{GB}} = 0.3$ μm was also tested and yielded a result of $\kappa_{latt} = 17.59$ W m^{-1} K^{-1} at 300 K. Both results for $L_{\mathrm{GB}} = 0.3$ and 0.5 μm are within the margin of error of the experimental value of $\kappa_{latt} \approx 17$ W m^{-1} K^{-1} (undoped NbFeSb, 12% relative error).

To complete the calculation, we include the effect of PD and EP interaction to κ_{latt}. The computation of the EP interaction requires knowledge of the electron τ. The lack of doping level dependence in the constant relaxation time approximation makes it unsuitable for calculating the EP contribution. The experimental data from the He *et al* study, including the temperature and doping dependencies, was used in accordance to the theoretical model and is discussed in more details in the supplementary materials. Figure 5(a) shows how the lattice thermal conductivity of $Nb_{1-x}Ti_xFeSb$ is reduced when all contributions are included. The results are presented for doping $x = 0.05$ and the best match to the experimental data is obtained with $L_{\mathrm{GB}} = 0.5$ μm. Figure 5(b) compares κ_{latt} when all contributions have been added to the experimental results. The computed

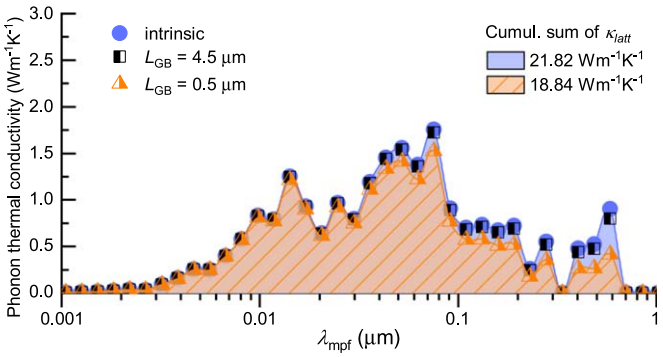

Figure 4. The impact of grain boundaries on the lattice thermal conductivity of NbFeSb at 300 K.

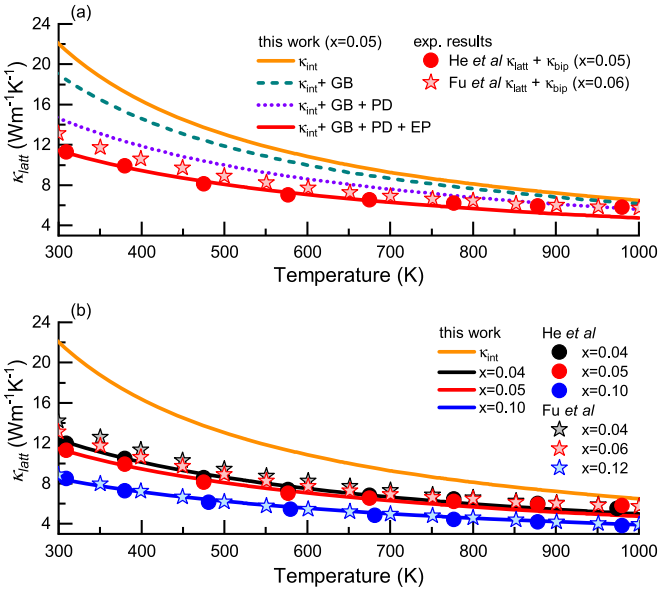

Figure 5. Figure (a) shows the contribution of grain boundaries GB, point defects PD and electron–phonon interaction EP to the lattice thermal conductivity κ_{int} of NbFeSb. Figure (b) compares the theoretical prediction of this study (solid lines) for $Nb_{1-x}Ti_xFeSb$ with $L_{GB} = 0.5$ μm to the experimental results (stars and circles).

values for the lattice thermal conductivity agree very well with the experimental study, particularly with the He *et al* study at temperatures of up to 700 K. There is a slight underestimate of the theoretical value of κ_{latt} at higher temperature for $x = 0.04$ and $x = 0.05$. This can be explained with the lack of a bipolar thermal conductivity (κ_{bip}) term in the calculations. In order to compute that, one needs to calculate a value for the electron relaxation time which depends on the doping level. Therefore, using the constant relaxation time approximation to compute κ_{bip} would yield inaccurate results. However, as it can be seen in figure 5(b), the contribution of κ_{bip} is sufficiently small that the computed values are still in a good agreement with the experimental measurements.

3.1.4. Figure of merit

The final results on the thermoelectric figure of merit ZT for the p-type $Nb_{1-x}Ti_xFeSb$ are presented in figure 6. A comparison between ZT values obtained in this study and the experimental data is shown in figure 6(a). There is a good agreement up to $T = 650$ K between our results and the measurements conducted by He *et al.* The overestimate of ZT above this temperature for $x = 0.04$ and 0.05 can be explained by the missing κ_{bip} term in the lattice thermal conductivity. This has already been discussed in the previous section and explains why the agreement between the experimental and theoretical results at high temperatures improves with the increase of the doping concentration. Additionally, the limitations of the constant relaxation time approximation, e.g. no dependence on the chemical potential and no inclusion of the extrinsic scattering mechanisms, can easily add up and lead to the observed discrepancies at lower temperatures. The results in this study slightly overestimate ZT when compared to Fu *et al* [4]. However, as with the lattice thermal conductivity results, there is a mismatch between the experimental results presented by He *et al* and Fu *et al.* The latter uses a much lower annealing

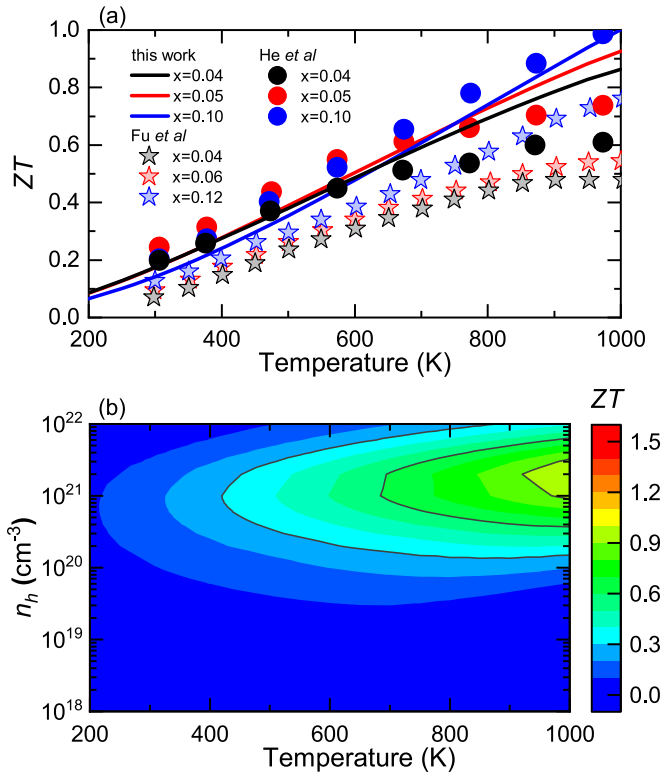

Figure 6. Comparison between our theoretical results and experimental measurements on *p*-type NbFeSb at $x = 0.04$, 0.05 and 0.10 (a). Subfigure (b) is a colour map which shows the ZT of *p*-type NbFeSb with respect to the charge carrier concentration and temperature, with a maximum ZT of 1 at $n_h = 2 \times 10^{21}$ cm^{-3} ($x = 0.1$) and $T = 1000$ K.

temperature, and so the density of the GB in the sample is expected to be higher. This further confirms that the constant relaxation time approximation could play a major role along with the bipolar term in the discrepancy between the theoretical and experimental results. The sample preparation in the Fu *et al* study influences both the electrical and thermal conductivity, and as a consequence, the measured ZT values are expected to be a bit lower than the ones obtained in our calculations.

The colour map in figure 6(b) shows that NbFeSb remains most efficient at high temperature, despite the big power factor of PF $= 9.3$ mW m^{-1} K^{-2} at 300 K. The *p*-doped NbFesb displays its best figure of merit ($ZT \approx 1.0$) at $T = 1000$ K and high doping levels between $x = 0.05$ and 0.10, corresponding to $n_h = 1 \times 10^{21}$ and 2×10^{21} cm^{-3}. This result is typical for half-Heusler alloys [23] and illustrates that a reduction of κ_{latt} can significantly enhance the thermoelectric performance of similar half-Heusler alloys.

3.2. TaFeSb

3.2.1. Electronic structure

The crystal structure of TaFeSb is very similar to NbFeSb with the only difference being the atomic species on the X-site. The lattice constant is calculated to be 5.95 Å. The band structure and DOS are presented in figure 7. The band gap of TaFeSb is calculated to be 0.86 eV, close to the value $\epsilon_g = 0.93$ eV computed by Bhattachrya and Madsen [9]. It can be seen that the valence bands and DOS near the Fermi level remain almost unchanged when compared to NbFeSb. This suggests that the *p*-type S, σ and κ_{el} should exhibit the same behaviour as in NbFeSb, leaving the relaxation time as the determining factor for any change in the electronic TE properties.

3.2.2. Electronic TE properties

The relaxation time along with the parameters necessary for its calculation are shown in table 2. There is a noticeable reduction in the DP values for both holes $V_{\mathrm{DP}} = -11.06$ eV (-13.98 eV for NbFeSb) and electrons $V_{\mathrm{DP}} = -11.81$ eV (-14.53 eV for NbFeSb). This means that stress has less effect on the electronic structure of TaFeSb. In addition, a slight reduction in the effective mass is also observed, with $m_h^* = 1.57(m_e)$. As a result, the mobility of the holes and relaxation time are increased to $\mu_h = 53.11$ cm^2 V^{-1} s^{-1} and $\tau_h = 47.32$ fs.

Next we present the electronic TE properties of TaFeSb in the form of colour maps in figure 8. The colour maps investigate a very wide doping and temperature range and might not be intuitive for comparison purposes. For that reason, we also provide 2D plots in figure 9, which compare the electronic properties of TaFeSb and NbFeSb for the common doping levels of $x = 0.04$, 0.05 and 0.10. The value of the *p*-type Seebeck coefficient for

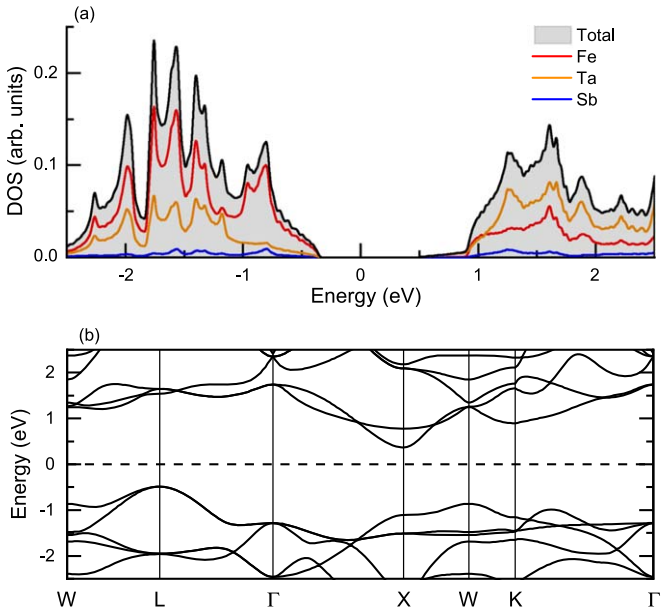

Figure 7. Density of states (a) and band structure (b) graphs of TaFeSb.

Table 2. Parameters needed for electron and hole τ calculations of TaFeSb. These include the deformation potential constant (V_{DP}), effective mass of charge carriers (m^*), carrier mobility (μ) and relaxation time (τ) at 300 K for electrons and holes.

Carrier type	V_{DP} (eV)	m^* (m_e)	μ (cm^2 V^{-1} s^{-1})	τ (fs)
Holes	−11.06	1.57	53.11	47.32
Electrons	−11.81	0.38	1 629.74	350.26

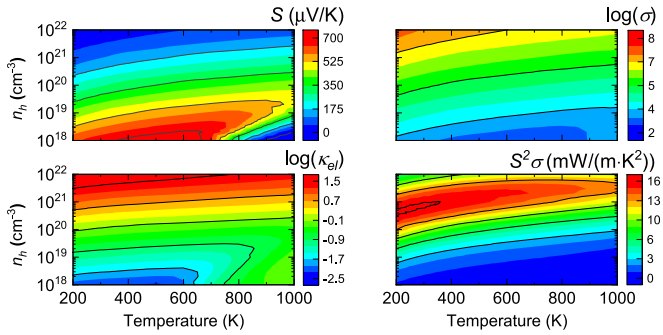

Figure 8. Colour maps of the electronic TE properties of *p*-type TaFeSb. The magnitude of the electrical conductivity σ (top right) and electronic thermal conductivity κ_{el} (bottom left) is given on a log scale. A maximum power factor (bottom right) value of PF $= S^2\sigma$ $= 16.11$ mW m^{-1} K^{-2} is obtained at 300 K and $n_h = 7 \times 10^{20}$ cm^{-3} ($x = 0.037$).

$x = 0.05$ is calculated to be 113.81 and 247.5 μV K^{-1} at 300 and 1000 K, respectively. The change in S with respect to the NbFeSb results for the same doping concentration is less than 1%, which is expected due to the similarity in the valence bands of both materials. On the other hand, the bigger band gap in TaFeSb results in a bigger *p*-type S at a very low doping concentration and temperature around 600 K. This is visualised with an increase of the red area in figure 8(a) when compared to NbFeSb in figure 2(a). The results confirm that not only does TaFeSb exhibit a competitive Seebeck coefficient around the experimentally investigated doping levels, but also shows a significant improvement at very low n_h and moderate T.

The results obtained from BoltzTraP for σ and κ_{el} predict a behaviour analogous to the changes observed for *p*-type S. Therefore, the increase of τ (holes), which is ≈80%, yields a significant improvement in σ, and an increase in κ_{el}. The increase of σ leads to an astonishing power factor of PF ≈ 16 mW m^{-1} K^{-2} at room temperature and $x = 0.03$–0.05. For comparison, the power factor of NbFeSb is estimated to be

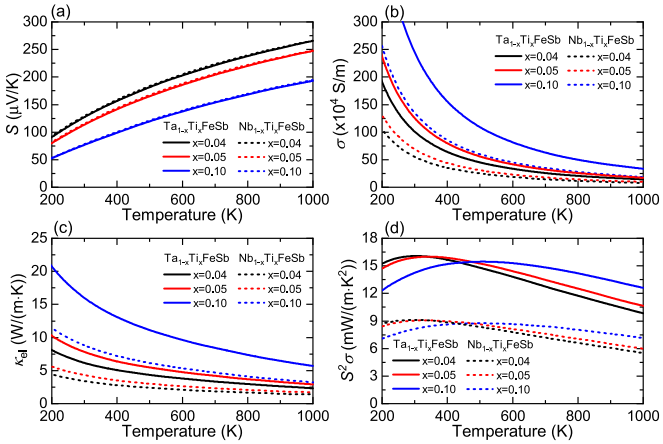

Figure 9. Comparison of the thermoelectric properties of TaFeSb and NbFeSb for $x = 0.04$, 0.05 and 0.10. The subfigures compare the Seebeck coefficient (a), electrical conductivity (b), electronic thermal conductivity (c), and power factor (d).

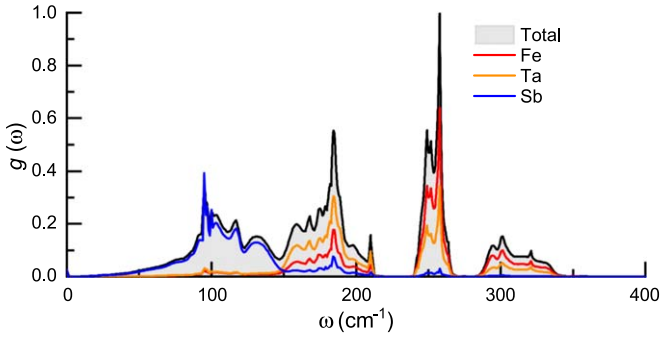

Figure 10. Phonon density of states of TaFeSb.

9–10 mW m^{-1} K^{-2}, and the maximum value for Fe_2VAl is measured to be 5.5 mW m^{-1} K^{-2} [24]. The compounds based on the already established TE material Bi_2Te_3 have a power factor between 1.5 and 6 mW m^{-1} K^{-2} [3, 25, 26]. The improvement in PF of TaFeSb over NbFeSb is maintained over a wide range of doping levels from $n_h = 10^{20}$ cm^{-3} to $n_h = 2 \times 10^{21}$ cm^{-3} and at higher temperatures (compare figures 8(d) and 2(d) and note the unchanged ranges). In summary, TaFeSb has a significantly better electronic TE performance than NbFeSb due to the increased band gap and higher mobility of the charge carriers.

3.2.3. Lattice thermal conductivity

The phonon DOS of TaFeSb, presented in figure 10, show a close resemblance to the NbFeSb results. There are no imaginary frequencies and so this structure is also mechanically stable. The data is again in a very good agreement with the results obtained by Zeeshan *et al* [12]. The low frequency region is up to 150 cm^{-1} and is dominated by Sb. The intermediate region between 150 and 220 cm^{-1} is due to Ta, instead of Nb. The last region is dominated by Fe atomic vibrations and occupies the high frequencies up to 350 cm^{-1}. It is also noticeable that a gap is formed in between the regions dominated by Ta and Fe. Our calculations show that the intrinsic value of κ_{latt} is 20.57 and 5.75 W m^{-1} K^{-1} at 300 and 1000 K, respectively. This is slightly lower than the NbFeSb results and can be accounted for by the gap between Ta and Fe in figure 10.

The effect of GB on κ_{latt} of TaFeSb at 300 K is shown in figure 11. GB of size 4.5 μm have an almost negligible effect on the lattice thermal conductivity. When their size is reduced to 0.5 μm κ_{latt} is computed to be 17.63 W m^{-1} K^{-1}. Although a similar behaviour was noticed in NbFeSb, the presence of an additional gap in the phonon DOS of TaFeSb leads to a different phonon mean free path λ_{mfp} distribution. A common dip in the phonon thermal conductivity is observed for both TaFeSb and NbFeSb between 0.3 and 0.4 μm. This can be explained by the common gap in the phonon DOS at $\omega \approx 275$ cm^{-1}. However, whilst the Ta–Fe gap in TaFeSb leads to an extra dip at 0.08 μm, this has a small effect as phonons with λ_{mfp} less than 0.3 μm contribute less to the total lattice thermal conductivity. Despite this difference, GB of the same size seem to reduce κ_{latt} in both

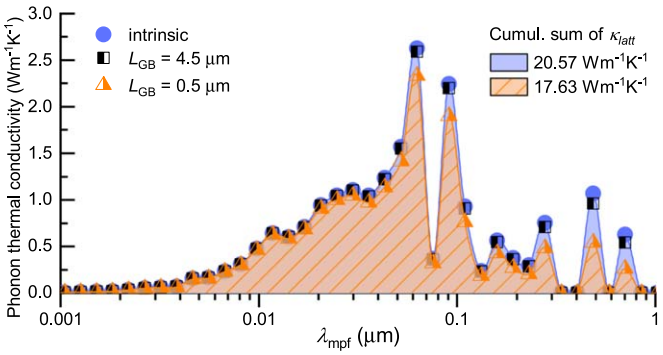

Figure 11. The impact of grain boundaries on the lattice thermal conductivity of TaFeSb at 300 K.

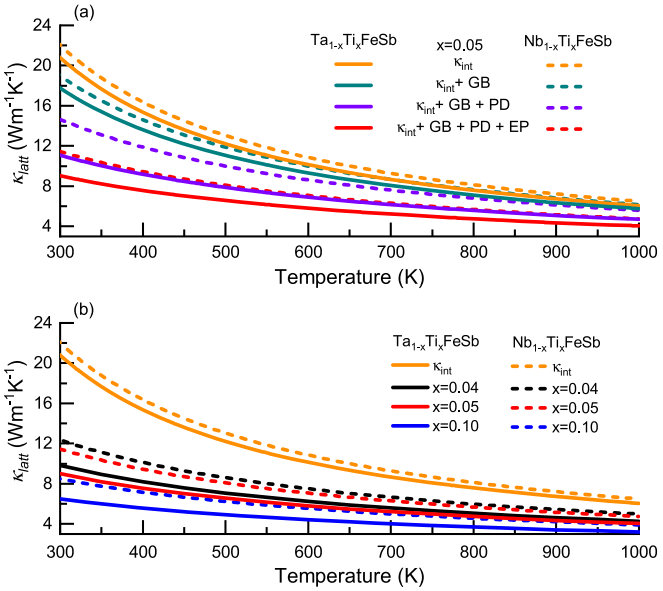

Figure 12. Figure (a) compares the lattice thermal conductivity of $Ta_{1-x}Ti_xFeSb$ (solid lines) and $Nb_{1-x}Ti_xFeSb$ (dashed lines) when the contribution of grain boundaries GB, point defects PD and electron–phonon interaction EP are added. The biggest change occurs when the contribution from point defects is added to the Ta-based compound. Figure (b) compares κ_{latt} with all contributions included at different doping levels.

TaFeSb and NbFeSb by a similar amount. This means that the change in the phonon mean free path distribution has an effect only on the intrinsic value of κ_{latt} but little impact on the effect of GB.

Next we proceed by adding the contribution of the PD due to Ti doping. The major difference between TaFeSb and NbFeSb is in the atomic mass of the X element. The mass of Ta is 180.95 amu, whereas Nb is significantly lighter with a mass of 92.906 amu. One of the crucial parameters in the Klemens model [22] for the thermal conductivity of systems with PD is the mass difference between the dopant atom (Ti) and the atoms which are substituted (Ta or Nb): a larger mass difference results in a greater reduction in the lattice thermal conductivity. Therefore, the lattice thermal conductivity of $Ta_{1-x}Ti_xFeSb$ is expected to be affected significantly by the Ti dopants. Figure 12(a) illustrates this point by comparing the $Ta_{1-x}Ti_xFeSb$ and $Nb_{1-x}Ti_xFeSb$ results. It is indeed seen that the reduction in κ_{latt} of the Ta-based compound due to PD (Ti doping) is much more significant. For $Nb_{1-x}Ti_xFeSb$ the lattice thermal conductivity is reduced by 23% and 9% at 300 K and 1000 K, respectively, when the PD are included. For $Ta_{1-x}Ti_xFeSb$ these numbers increase to 37% and 18% at 300 K and 1000 K, respectively.

The last contribution which needs to be added is the EP interaction. As already described, it is meaningless to use the constant relaxation time approximation to compute the EP interaction. For that reason, experimental data was used earlier to obtain a value for the NbFeSb compound. Unfortunately, there are no experimental measurements which can be used to extract a value for the EP contribution in TaFeSb. For practical purposes and because of the similarity in the electronic structure and phonon DOS between TaFeSb and NbFeSb, we will

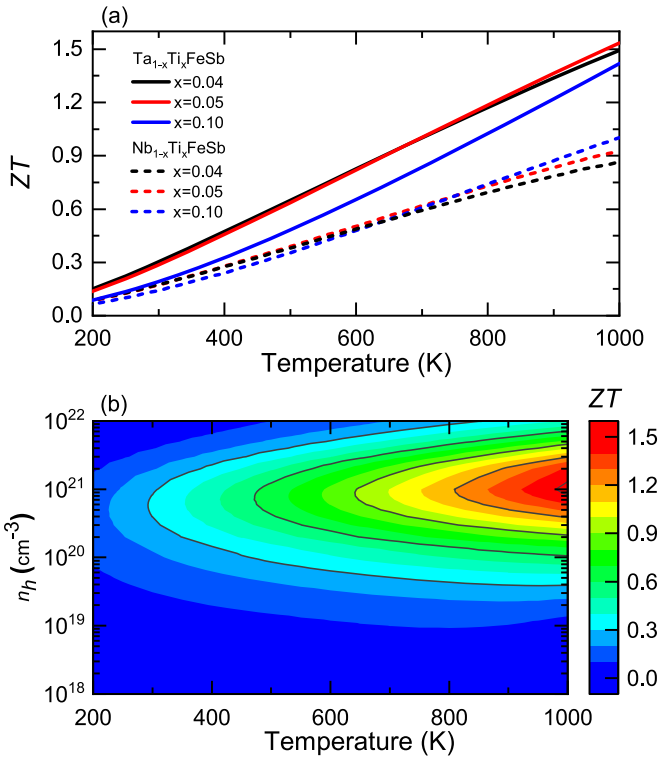

Figure 13. Comparison between *p*-type TaFeSb and NbFeSb at $x = 0.04$, 0.05 and 0.10 (a). Subfigure (b) is a colour map which shows the *ZT* of *p*-type TaFeSb with respect to the charge carrier concentration and temperature, with a maximum *ZT* of 1.53 at $n_h = 1 \times 10^{21}$ cm^{-3} ($x = 0.05$) and $T = 1000$ K.

use the EP contribution which was extracted for NbFeSb. In the worst case, such an approximation would lead to an overestimate of κ_{latt} and an underestimate of the *ZT* of TaFeSb rather than the opposite.

Figure 12(b) shows the lattice thermal conductivity of $Ta_{1-x}Ti_xFeSb$ and $Nb_{1-x}Ti_xFeSb$ at different doping levels with all contributions included. The trend shows that κ_{latt} of the Ta-based compound is lower at all doping levels. At $x = 0.05$, κ_{latt} is lower by 21% ($\kappa_{latt} = 8.99$ W m^{-1} K^{-1}) and 15% ($\kappa_{latt} = 4.04$ W m^{-1} K^{-1}) at 300 K and 1000 K, respectively. At $x = 0.10$, the reduction is 23% ($\kappa_{latt} = 8.43$ W m^{-1} K^{-1}) and 18% ($\kappa_{latt} = 3.20$ W m^{-1} K^{-1}) at 300 K and 1000 K, respectively. The improvement of 15%–23%, as already discussed, comes from the slightly lower intrinsic value of κ_{latt} for TaFeSb and the bigger mass difference between Ta and Ti. There is also a noticeable similarity of the lattice thermal conductivity of $Ta_{1-x}Ti_xFeSb$ at $x = 0.05$ and that of $Nb_{1-x}Ti_xFeSb$ at $x = 0.10$. This hints that TaFeSb might require less doping than NbFeSb to reach its maximum *ZT* value.

3.3. Comparison between *ZT* of *p*-type TaFeSb and NbFeSb

Finally, we present the results on *ZT* of $Ta_{1-x}Ti_xFeSb$ and compare them to the $Nb_{1-x}Ti_xFeSb$ results. Figure 13 shows that the maximum thermoelectric figure of merit is obtained at $T = 1000$ K, $x = 0.05$ and is equal to $ZT = 1.53$. For comparison the maximum *ZT* value for $Nb_{1-x}Ti_xFeSb$ is only 1.01, and at $x = 0.10$. Figure 13(a) shows that $Ta_{1-x}Ti_xFeSb$ exhibits higher *ZT* across the entire temperature range and at all doping levels. The main difference to $Nb_{1-x}Ti_xFeSb$ is that there is a 50% increase in *ZT* and that the peak is achieved at $x = 0.05$ rather than $x = 0.10$, which is in agreement with the prediction made in the lattice thermal conductivity section.

The colour map in figure 13(b) reveals a broad area between 800 and 1000 K, and $x = 0.02$ and $x = 0.15$ in which the *ZT* of $Ta_{1-x}Ti_xFeSb$ is higher than 1.2. At moderate temperature (500–700 K) the *ZT* value drops to $\approx$1, which is still considered as an excellent TE result. Even at room temperature, the TE figure of merit ($ZT = 0.3$) is almost two times bigger than that of NbFeSb ($ZT = 0.17$). The wide range of conditions, which result in a good *ZT* value, suggests that *p*-type TaFeSb can indeed be used as a novel material for efficient thermoelectric devices.

4. Conclusions

We have conducted a thorough study of the thermoelectric properties of *p*-type NbFeSb and TaFeSb. In addition to solving the BTEs for electrons and phonon with *ab initio* inputs, several approximations were also included in

the process. These are the constant relaxation time approximation with no dependence on the chemical potential due to doping, the choice of GB size and the inclusion of the EP interaction based on experimental data. This multi-step procedure needs to be executed with caution, and so at each step the results have been thoroughly compared to the available experimental measurements. We would like to point out that although the results in this study look promising and are consistent with the expectations, one should not use the presented theoretical framework lightly on fully unknown compounds. The key feature of this study was to preserve the chemical environment of NbFeSb and change it slightly to TaFeSb in a way that the empirical Klemens' equation is still applicable.

In summary, the NbFeSb results agree extremely well with multiple theoretical and experimental studies. The same procedure was then used to perform a full-scale computation on the TE properties of TaFeSb. The results have shown that both compounds exhibit high power factor at room temperature and have a good thermoelectric figure of merit at high temperatures. At 1000 K we find PF $= 9$ mW m^{-1} K^{-2} and $ZT = 1$ for NbFeSb and PF $= 16$ mW m^{-1} K^{-2} and $ZT = 1.5$ for TaFeSb. The higher atomic mass of Ta (compared to Nb) increases the scattering strength in Ti-doped TaFeSb, which reduces the lattice thermal conductivity of the compound. At the same time, *p*-type charge carries in TaFeSb exhibit higher mobility and relaxation time, which increases the power factor. The net result is a material with an amazing power factor of 16 mW m^{-1} K^{-2} and ZT value which is approximately 50% better than that of NbFeSb.

In conclusion, TaFeSb not only appears to be a better TE material than NbFeSb, but it also opens a new path of TE optimisation of materials based on the two alloys. In theory, an alloy based on $Nb_{1-x}Ta_xFeSb$ should exhibit good electrical properties due to the similarities in the electronic structure of NbFeSb and TaFeSb. At the same time, the mass difference between Nb and Ta should create additional scattering centres which would suppress the lattice thermal conductivity even before doping, and so the final doped compound should exhibit an even higher ZT value. This is further hinted by a very recent experimental study by Yu *et al* [8], which reports the successful synthesis of $Nb_{1-x}Ta_xFeSb$ alloys and a measured ZT of up to 1.6.

Acknowledgments

PJH acknowledges financial support from EPSRC (Grant Ref. EP/R025770/1). We are grateful for computational support from the UK national high performance computing service, ARCHER, for which access was obtained via the UKCP consortium and funded by EPSRC Grant Ref. EP/P022561/1.

ORCID iDs

G A Naydenov https://orcid.org/0000-0002-5403-8405
P J Hasnip https://orcid.org/0000-0002-4314-4093
V K Lazarov https://orcid.org/0000-0002-4314-6865
M I J Probert https://orcid.org/0000-0002-1130-9316

References

[1] He R *et al* 2016 *Proc. Natl Acad. Sci. USA* **113** 13576
[2] Tavassoli A, Failamani F, Grytsiv A, Rogl G, Heinrich P, Müller H, Bauer E, Zehetbauer M and Rogl P 2017 *Acta Mater.* **135** 263
[3] Wu F, Wang W, Hu X and Tang M 2017 *Prog. Nat. Sci.: Mater. Int.* **27** 203
[4] Fu C, Zhu T, Liu Y, Xie H and Zhao X 2014 *Energy Environ. Sci.* **8** 216
[5] Hong A J, Li L, He R, Gong J J, Yan Z B, Wang K F, Liu J-M and Ren Z F 2016 *Sci. Rep.* **6** 22778
[6] Fang T, Zheng S, Chen H, Cheng H, Wang L and Zhang P 2016 *RSC Adv.* **6** 10507
[7] Fang T, Zheng S, Zhou T, Yan L and Zhang P 2017 *Phys. Chem. Chem. Phys.* **19** 4411
[8] Yu J, Fu C, Liu Y, Xia K, Aydemir U, Chasapis T C, Snyder G J, Zhao X and Zhu T 2018 *Adv. Energy Mater.* **8** 1701313
[9] Bhattacharya S and Madsen G K H 2016 *J. Mater. Chem.* C **4** 11261
[10] Zhang X, Wang Y, Yan Y, Wang C, Zhang G, Cheng Z, Ren F, Deng H and Zhang J 2016 *Sci. Rep.* **6** 33120
[11] Zhu H *et al* 2019 *Nat. Commun.* **10** 270
[12] Zeeshan M, Nautiyal T, van den Brink J and Kandpal H C 2018 *Phys. Rev. Mater.* **2** 065407
[13] Clark S J, Segall M D, Pickard C J, Hasnip P J, Probert M I J, Refson K and Payne M C 2005 *Z. für Kristallogr.—Cryst. Mater.* **220** 567
[14] Perdew J P, Burke K and Ernzerhof M 1996 *Phys. Rev. Lett.* **77** 3865
[15] Lejaeghere K *et al* 2016 *Science* **351** aad3000
[16] Monkhorst H J and Pack J D 1976 *Phys. Rev.* B **13** 5188
[17] Morris A J, Nicholls R J, Pickard C J and Yates J R 2014 *Comput. Phys. Commun.* **185** 1477
[18] Madsen G K H and Singh D J 2006 *Comput. Phys. Commun.* **175** 67
[19] Bardeen J and Shockley W 1950 *Phys. Rev.* **80** 72
[20] Refson K, Tulip P R and Clark S J 2006 *Phys. Rev.* B **73** 155114
[21] Li W, Carrete J, Katcho N A and Mingo N 2014 *Comput. Phys. Commun.* **185** 1747–58
[22] Madarasz F L and Klemens P G 1987 *Int. J. Thermophys.* **8** 257

[23] Rull-Bravo M, Moure A, Fernández J F and Martín-González M 2015 *RSC Adv.* **5** 41653
[24] Nishino Y 2011 *IOP Conf. Ser.: Mater. Sci. Eng.* **18** 142001
[25] Kim J-H, Choi J-Y, Bae J-M, Kim M-Y and Oh T-S 2013 *Mater. Trans.* **54** 618
[26] Ovsyannikov S V, Shchennikov V V, Vorontsov G V, Manakov A Y, Likhacheva A Y and Kulbachinskii V A 2008 *J. Appl. Phys.* **104** 053713